Recoverable impacts of ocean acidification on the tubeworm, *Hydroides elegans*: implication for biofouling in future coastal oceans

Yuan Meng[a], Chaoyi Li[a], Hangkong Li[b], Kaimin Shih[b], Chong He[c], Haimin Yao[c] and V. Thiyagarajan[a,d]*

[a]*The Swire Institute of Marine Science and School of Biological Sciences,* [b]*Department of Civil Engineering, The University of Hong Kong, Hong Kong SAR, China;* [c]*Department of Mechanical Engineering, The Hong Kong Polytechnic University, Hong Kong SAR, China;* [d]*State Key Laboratory for Marine Pollution, Hong Kong SAR, China*

*Corresponding author (V. Thiyagarajan: rajan@hku.hk)

Recoverable impacts of ocean acidification on the tubeworm, *Hydroides elegans*: implication for biofouling in future coastal oceans

Ocean uptake of anthropogenic CO_2 causes ocean acidification (OA), which not only decreases the calcification rate, but also impairs the formation of calcareous shells or tubes in marine invertebrates such as the dominant biofouling tubeworm species, *Hydroides elegans*. This study examined the ability of tubeworms to resume normal tube calcification when returned to ambient pH 8.1 from a projected near-future OA level of pH 7.8. Tubeworms produced structurally impaired and mechanically weaker calcareous tubes at pH 7.8 compared to at pH 8.1, but were able to recover when the pH was restored to ambient levels. This suggests that tubeworms can physiologically recover from the impacts of OA on tube calcification, composition, density, hardness and stiffness when returned to optimal conditions. These results add to our understanding of the progression of biofouling communities dominated by tubeworms in future oceans with low pH induced by OA.

Keywords: Biofouling; calcification; ocean acidification; micro-CT scanning; *Hydroides elegans*

1. Introduction

Calcareous tube-forming marine invertebrates such as the polychaete tubeworm, *Hydroides elegans,* are one of the most important habitat-forming species in warm tropical waters (Underwood 1999). Free-swimming larvae of marine invertebrates must find favourable sites for settlement and attachment for subsequent metamorphosis into adults. However, tubeworm species often attach to fishing nets and other submerged man-made structures, which is a major concern from a biofouling control perspective (Watson et al. 2009). Immediately after attachment, tubeworms construct calcareous tubes by incorporating Ca^{2+} and CO_3^{2-} ions from the seawater into a complex organic-inorganic matrix by physiologically controlled calcification and biomineralization process (Vinn et al. 2009; Tanur et al. 2010; Vinn & Kupriyanova 2011; Meng et al. 2018). In marine environments, calcification is not only controlled by internal processes but is also affected by external environmental factors such as pH, concentrations of carbonate ions and their saturation levels (Orr et al. 2005; Solomon et al. 2007). The increasing uptake of anthropogenic CO_2 by coastal and open oceans is not only decreasing the pH and shifting the equilibrium of the carbonate system through the well-known process of ocean acidification (OA), but is also increasing the magnitude of daily (and seasonal) fluctuations of these variables (Doney et al. 2009; Feely et al. 2009). Estuarine and coastal waters are particularly vulnerable to OA, and the effects on calcifying species has become a topic of interest in biofouling literature (McDonald et al. 2009; Peck et al. 2015; Nardone et al. 2018, Dobretsov et al. 2019).

Several short-term studies have demonstrated that OA significantly affects the calcification process and/or its products (shell or tube) of major biofouling species such as barnacles, tubeworms and oysters. Their response to OA is not only highly species-specific, but also dependent on the developmental stage (Ries et al. 2009). For example, the larval stages of both

barnacles and tubeworms show no response to the near-future OA level of pH 7.7, possibly because their larval stages calcify much less than their sessile adult stages (Pansch et al. 2012; Espinel-Velasco et al. 2018). The intertidal barnacle species, *Amphibalanus amphitrite,* was found to be robust to reduced pH (7.78 and 7.50) (Nardone et al. 2018) and even increased its exoskeleton calcification at pH 7.4 (McDonald et al. 2009). Some species are able to mitigate the effects of OA through compensatory physiological adjustments during the calcification process (Wood et al. 2008; Thomsen et al. 2010). For example, oysters tend to alter their shell microstructure to cope with OA-induced dissolution of calcium carbonate polymorphs at pH 7.4 (Beniash et al. 2010; Asnaghi et al. 2014; Meng et al. 2018), whereas corals, *Stylophora pistillata,* and foraminifera, *Ammonia* sp., modulate their intercellular pH levels at the tissue-skeleton interfaces to survive under OA (Holcomb et al. 2014; Hendriks et al. 2015; Toyofuku et al. 2017). Consequently, mitigating the effects of OA may lead to energy trade-offs between calcification, physiological development and reproduction at the expense of other traits (Wood et al. 2008; Lannig et al. 2010; Ivanina et al. 2017; Meng et al. 2019). On the other hand, adult tubeworms have been shown to be sensitive to the projected near-future OA level of pH 7.8, resulting in decreased calcification rates, and structurally impaired and mechanically weaker tubes (Chan et al. 2012; Li et al. 2014). These weaker tubes would not only make tubeworms more vulnerable to predation, but also would decrease the intensity of biofouling communities in topical waters (Fitridge et al. 2012).

However, most of studies looking at responses of biofouling species to OA have focused on the effects of exposure to a constant pH level. In particular, pH variability in coastal areas can be much greater than in the open ocean due to diurnal fluctuations, upwelling of nutrients, photosynthesis and microbial activities (Wootton et al. 2008; Borgesa & Gypensb 2010; Cai et al. 2011; Howarth et al. 2011). Therefore, biofouling species living in coastal or estuarine

environments with highly fluctuating pH levels may have developed adequate physiological plasticity to tolerate extreme decreased pH levels, similar to OA conditions (Baumann et al. 2015). This strong acclamatory capacity may help these populations survive under OA. In other words, previously observed immediate negative effects of OA on some biofouling species may only be a temporary short-term response, which can be reversed if favourable conditions return. The recovery potential of a species is important to correctly predict the near-future impacts of OA (Ghalambor et al. 2007; Gienapp et al. 2008; Dupont & Thorndyke 2009). However, there are still significant knowledge gaps in our understanding of the acclamatory mechanisms and recovery effectiveness of marine bio-calcifiers to the effects of OA, especially environmental resilience with respect to calcification products such as shell chemical composition, mechanical properties and predation protection.

This study investigated how the current ambient pH 8.1 and near-future OA level of pH 7.8 affect the construction of calcareous tubes of the dominant biofouling serpulid tubeworm, *Hydroides elegans,* and whether this species has adequate physiological plasticity to recover from the effects of decreased pH after returning to an ambient pH environment (Yuan et al. 2011). We hypothesize that the impact of OA on the structural and mechanical properties of the tubes of *Hydroides elegans* will be fully reversible when favourable ambient pH conditions return.

2 Materials and methods

2.1 Test animal

Adult *Hydroides elegans* were collected from floating structures in fish farms in Hong Kong (22°27′N, 114°23′W) in December 2014 (ambient conditions: ~20°C, salinity 34 psu, and pH 8.1). Animals were acclimatized in the laboratory for 2 days in an ambient temperature, pH and salinity condition. The eggs and sperms were obtained from over 100 randomly selected individuals and

mixed in filtered seawater (FSW, 0.25 µm) for fertilization. After 2 hours, embryos were cleaned in FSW and collected in a 20-µm mesh for use in the following pH perturbation experiment. Further details about the test animals, collection sites and procedures for larval and adult tubeworm cultures used in this study are available in our previous papers (Chan et al. 2012; Chan et al. 2013; Lane et al. 2013; Li et al. 2014; Li et al. 2016).

2.2 Experimental design

Seawater pH was used as a proxy to investigate carbonate system variability in response to perturbations induced by high CO_2, namely ocean acidification (OA). Embryos of *Hydroides elegans,* at a density of 10 per mL in 1-L tanks, were subject to various pH treatments as a proxy for these OA changes. The treatments included two levels of pH: ambient pH 8.1 (control pH treatment) and pH 7.8 (decreased pH treatment). The decreased pH treatment represents (1) the average variation in pH experienced by the tubeworm species inhabiting Hong Kong (Yuan et al. 2011), and (2) the average near-future seawater pH, which is projected to decrease by 0.3 units from ambient pH 8.1 to 7.8 within this century due to ocean acidification (Duarte et al. 2013). The experimental design consisted of two stages (Figure 1), stage 1: 0-30 days ('0' denotes the date of settlement) and stage 2: 30-60 days. Tubeworms (4 replicates for each condition) were subject to the various pH treatments at each stage, respectively. Tubeworms were cultured under ambient control conditions at pH 8.1 or decreased pH conditions at pH 7.8 according to the procedures describe in our previous papers (Chan et al. 2012; Li et al. 2014). In total, there were four treatment groups across the two stages: CC group (stage 1: pH 8.1, stage 2: pH 8.1), CT group (stage 1: pH 8.1, stage 2: pH 7.8), TC group (stage 1: pH 7.8, stage 2: pH 8.1) and TT group (stage 1: pH 7.8, stage 2: pH 7.8). Plastic sheets pre-cultured with 7-day-old biofilms were used for the settlement and attachment of tubeworm larvae on day 6 of stage 1. Animals were fed and maintained using

the procedures described in previous papers (Chan et al. 2012; Lane et al. 2013; Li et al. 2014). The pH level in each tank was maintained according to the assigned experimental groups following standard OA procedures as described previously (Lane et al. 2013). Briefly, ambient pH 8.1 was lowered to pH 7.8 by directly bubbling air enriched with CO_2. The required CO_2 concentration was controlled by high-resolution gas flow meters/controllers (Cole-Parmer, USA). Seawater pH (at NBS scale) and temperature were measured using a Metter-Toledo (SG2) probe and salinity was measured using a refractometer (S/Mill-E; ATAGO, Japan). Daily measurements of pH, temperature and salinity were averaged within and among days for each replicate to reflect the experimental condition in each tank (mean ± SD; Table S1). Total alkalinity (TA) measurements were made using an Alkalinity Titrator (AC-A2; Apollo SciTech Inc., U.S.). The carbonate system parameters including carbon dioxide partial pressure (pCO_2; µatm), carbonate ion concentration (CO_3^{2-}; µmol kg^{-1}), and calcite and aragonite saturation states (Ω_{Ca}, Ω_{Ar}) were calculated using the CO2SYS software program (Pierrot et al. 2006) with equilibrium constants K_1, K_2 and KSO_4 (Mehrbach et al. 1973; Dickson & Millero 1987) (Table S1). On day 60, tubes were cleaned with MilliQ water and preserved in 70% ethanol at room temperature (Clode et al. 2011). Tubes were air-dried at room temperature for use in the following analyses.

2.3 Tube growth rate measurements

Tube growth in the different stages was determined by measuring the tube length on day 30 and day 60 for all treatment groups. The substrates were taken out from the culturing tanks for tube measurements before the water conditions were changed. Substrates together with a standardized scale bar were observed under a compound microscope equipped with a digital camera (Leica DFC 280, Leica, Germany). The length of each tube was measured from the posterior end to the anterior opening (Figure 1) using ImageJ software (1.49V, National Institutes of Health, USA) within 60

seconds to prevent any damage due to water evaporation. The tube length data at each stage served as the reference for tube growth in the different treatment groups. Sectioned tube portions from stage 1 and stage 2 were used in the following experiments and analyses (Figure 1a).

2.4 Determination of calcium carbonate polymorph proportions

X-ray Diffraction (XRD) and Fourier transform infrared spectroscopy (FTIR) were used to quantitatively and semi-quantitatively determine the proportion of the two calcium carbonate polymorphs, calcite and aragonite, which are the main components that make up the tubes. The protocols followed the procedures described in previous studies (Chan et al. 2012). The stage 1 and stage 2 tube sections obtained from each treatment (CC, CT, TC and TT) were analysed separately. Briefly, 10-25 tubeworms from each replicate (n=3-4 for each stage) were gently detached from the substrates and submerged in 70% ethanol. Tubes rinsed in MilliQ water were air-dried and ground into a fine powder for use in the following analyses.

The X-ray diffraction pattern of the powered tube samples was acquired using a Bruker D8 Advanced X-ray powder diffractometer (Bruker, USA) with a CuKα radiation generator and a LynxEye sensor (Chan et al. 2012), and standardized parameters: 40 kV, 40 mA, a 2θ scan range of 10^{o} to 110^{o}, step size of 0.02^{o} and a scan speed of 0.3 s/step. A Standard Reference Material 660a (lanthanum hexaboride, LaB6, U. S. National Institute of Standard and Technology, USA) was used to calibrate the XRD system. Eva XRD Pattern Processing software (Bruker, USA) was used to analyse the $CaCO_3$ mineral phases of the tubes by powder diffraction pattern matching using the standard database of the International Centre for Diffraction Data (ICDD PDF-2 Release 2008). TOPAS (version 4.0) crystallographic program was employed for the quantitative analysis of the mineral phase compositions using the Rietveld refinement method.

The powered tube samples were also examined by FTIR. Samples (~1 mg) were mixed with KBr (~10 mg; dehydrated at 98°C overnight) and pressed into a 13-mm diameter pellet (9 tons for 2 min). The powder spectrum (500-2000 cm^{-1} with 1 cm^{-1} resolution) was obtained using a Fourier transform infrared spectrometer (L120-000B; Perkin Elmer, USA). The relative proportions of carbonate polymorphs (calcite/aragonite) and the organic matrix content in the tubes were determined by comparing with standardized calcium carbonate IR peaks in the FTIR database (Chan et al. 2012).

2.5 Spatial density and 3D surface topography measurements

A micro-computed tomography (micro-CT) scanning system (SkyScan 1076, Skyscan, Belgium) with a $3x10^{-6}$ cubic mm voxel size and a spatial resolution of 15 μm was used to obtain the spatial 3D topography images and density heat map (Li et al. 2014). About 2-4 tubes per replicate (CC, CT, TC, and TT) in falcon tubes were stabilized and transferred into the micro-CT chamber for X-ray scanning. Tube density data was acquired by relative comparison with two imaging phantoms using an established universal scanning signal threshold. Shell densities were calculated by relative comparison using standardized phantoms for bone density measurements in the analytical software CT-Analyser v 1.14.4.1 (SkyScan; Kontich, Belgium) (Celenk & Celenk 2012). Images (89-322 per sample) were acquired to obtain a 3D model (SkyScan) that was reconstructed using CTvol software (v 2.2.1.0). CTvol can be used to generate 3D models with longitudinal inner sections by using the top-cut function, and the colours indicate changes in the density distribution.

2.6 Spatial hardness and stiffness measurements

Samples used in the non-destructive Micro-CT analysis were also used for the nanoindentation measurements (Li et al. 2014). Multiple nanoindentations using a Berkovich tip (TI 900; Hysitron, MN, USA) were made in the longitudinal direction of the apical region of the tubes to measure the

hardness and stiffness from posterior end (normalized length of 0) to anterior opening (normalized length of 1). For each treatment condition (CC, CT, TC, and TT), 5-12 indentations at the same interval were performed on the tubes of 3-6 tubeworms. The peak load used in the indentation process was 10 mN based on our previous work (Li et al. 2014).

Four respective maps of hardness and stiffness were generated from the indentation data for each treatment. Normalized hardness and stiffness were acquired by dividing the obtained hardness and stiffness values by the mean of all the indents in a replicate, where '1' denotes the average hardness and stiffness of the tube development. Each data point on the map represents an individual indentation at one location in a longitudinal direction of the tube, and all indentation plots were collected to generate the final maps. Mechanical properties, in terms of hardness and stiffness, were calculated according to the loading-unloading curve at each indentation using the Oliver-Pharr model (Doerner & Nix 1986; Oliver & Pharr 1992).

2.7 Statistical analyses

All data were subject to parametric homogeneity of variance and normality assumption tests before analysis by student's t-test. Data sets that did not meet the requirements for parametric t-tests, such as mineral density, were analysed by Mann-Whitney U tests. Tube length and C/A ratios of stage 1 sections between CC and CT groups, and between TC and TT groups were firstly compared using student's t-test. There should be no differences between stage 1 tubes in control conditions or between stage 1 tubes under treatment conditions. When no significant difference was found, then the effect of decreased pH could be tested by comparing between stage 1 tubes raised under the control conditions (stage 1 sections of CC and CT) and those in decreased pH conditions (stage 1 sections of TC and TT) using student's t-test (Figure 1). The recovery ability of tubes was tested by comparing the data of stage 2 sections between TC and CC groups. Linear and exponential

functions were fitted to the normalized lengths (0 = posterior end; 1 = anterior opening) versus normalized hardness and stiffness, and the significance of the fit (*p* value) and the % variance explained by the line (R^2) were compared as in (Dickinson et al. 2013).

3. Results

3.1 Effect of decreased pH on tube size, a proxy of calcification

The tube total length was measured before the treatment conditions were changed on day 30 and then final measurements were made on day 60 (Figure 1). In stage 1, calcification rate was significantly reduced at pH 7.8 (TC group) compared to the control (CC group) after 30 days of post-metamorphosis exposure (Figure 2a). However, there was no significant difference in tube lengths between CC and TC groups during the stage 2 "recovery" exposure (Figure 2b), meaning the calcification rate of the TC group recovered to that of the control group upon changing back to ambient pH levels. Similarly, there was no significant difference in tube lengths at stage 1 between CC and CT groups as well as between TC and TT groups (Table S2).

3.2 Effect of decreased pH on the chemical (mineral) composition of tubes

X-ray diffraction and FTIR spectroscopy were used to analyse the effects of pH on tube mineral composition. The XRD results showed changes in the proportions of the two $CaCO_3$ mineral forms in response to decreased pH. Tubes grown at pH 7.8 showed a significantly higher calcite/aragonite (C/A) ratio compared to the control during stage 1 (Figure 3a). However, there was no significant difference in C/A ratios of stage 2 individuals in the CC and TC groups (Figure 3b). These results indicate the tubes of the TC group recovered back to the same mineral composition as the CC group after conditions reverted back to ambient pH levels. There was no significant difference in C/A ratio at stage 1 between CC and CT groups as well as between TC and TT groups (Table S2).

The FTIR analysis showed the tubes built by tubeworms in all four treatment groups had both inorganic and organic matrices, regardless of the pH treatments (Figure 4). The FTIR spectra showed IR bands at 1644 cm^{-1} attributed to C=O stretching (amide I) groups and at 1158 cm^{-1} attributed to C–C stretching groups, which were both related to the organic content of the tubes. The carbonate ion content in the tubes was demonstrated by the presence of internal vibration modes of the CO_3^{2-} ions: ν_4 (700 cm^{-1} and 714 cm^{-1}), ν_2 (860 cm^{-1} and 874 cm^{-1}), ν_1 (1082 cm^{-1}), and ν_3 (1429 cm^{-1} and 1496 cm^{-1}). Specifically, IR bands around 700, 860 and 1082 cm^{-1} are characteristic of aragonite structures, whereas IR bands around 874 and 1429 cm^{-1} are characteristic of calcite structures. IR bands around 714, 1496 and 1788 cm^{-1} are common features of CO_3^{2-} compounds that can indicate both types of calcium polymorphs. A calcite peak at 874 cm^{-1} was evident in the spectra of tubes built at pH 7.8 during stage 1 compared to the control (Figure 4a), which indicates increased formation of calcite at pH 7.8 over other mineral forms. In stage 2, the peaks of the spectra of the TC group were similar to that of the CC group (Figure 4b), which indicated the tubes cultured at pH 7.8 recovered their normal mineral composition after switching back to the control conditions.

3.3 Effect of decreased pH on mineral density distribution

The comparative visual analysis of the 3D tube density maps clearly showed the tubes in the TC group started to accumulate high density minerals after switching back to the control condition from the decreased pH condition (Figure 5a-c). In addition, three types of tube construction were analysed: tube construction without density map (Figure 5a), construction with full-density map (Figure 5b), and construction with only high-density portions (Figure 5c, density > 0.5 g/cm^3). The ‘pores’ or ‘disconnections’ in the maps are regions where the mineral density is either lower than the detectable threshold of the micro-CT system (Figure 5a and b) or lower than 0.5 g/cm^3, which

were excluded as low-density portions (Figure 5c). As shown in Figure 5c, both the CC and CT groups had large high-density areas close to the posterior end (density ≥ 0.5 g/cm^3), suggesting the tubeworms constructed tubes with more densely packed minerals during stage 1 under ambient conditions (CC and CT groups), whereas the structures were partially impaired by decreased pH (TC and TT groups). However, CC and TC groups showed similar well-structured tubes close to anterior opening at stage 2, whereas CT and TT groups had tubes with more 'pores' (Figure 5c), indicating tubes recovered their mineral density after switching back to the control conditions.

The micro-CT analysis of stage 1 (Figure 5d) and stage 2 (Figure 5e) samples clearly showed the tube mineral density significantly decreased in response to decreased pH compared to the controls (Figure 5d). However, there was no significant difference in tube mineral density between CC and TC groups during the stage 2 "recovery" exposure (Figure 5e). Similarly, there was no significant difference in tube density at stage 1 between CC and CT groups as well as between TC and TT groups (Table S2).

3.4 Response of hardness and stiffness distribution to decreased pH

The nanoindentation test was used to quantitatively compare the mechanical properties of tubes after stage 1 and 2 treatments. The correlation analysis between the normalized tube length (including tube portions built at stage 1 and stage 2) and normalized mechanical properties (hardness and stiffness) for all four treatment groups is shown in Figure 6. The visual analysis of the data distribution as well as the corresponding statistical analysis of the data correlation revealed three types of responses. First, there was a positive relationship pattern for CC and TT groups (Figures 6a and d) of an increasing trend in both hardness and stiffness as a function of time of exposure (tube length) in both stage 1 and 2. In both CC and TT groups, tube mechanical properties continued to increase with tube length from the start of stage 1 to the end of stage 2 (Figure 6a and

d). Notably, tube hardness and stiffness in the TT group increased two times faster compared to the CC group, as demonstrated by a regression line slope of 0.8 in the CC group compared to 1.9 in the TT group (Table S3). Second, the CT group showed a neutral pattern with no clear relationship between exposure stage and mechanical properties (Figure 6b). The CT group showed a slight increasing trend in hardness in the ambient pH of stage 1, but this reversed to a decreasing trend in hardness in newly formed tubes when switching to decreased pH in stage 2 (Figure 6b). Finally, a positive threshold pattern was observed for the TC group, with no correlation or significant changes in the mechanical properties observed during stage 1, but a positive relationship between hardness and tube length was seen at stage 2 (Figure 6c). Interestingly, both the hardness and stiffness of tubes in the TC group increased dramatically with tube growth during the "recovery" exposure in stage 2 (Figure 6c). In general, correlation patterns of hardness and stiffness with normalized tube length were identical regardless of the pH treatment.

4. Discussion

This controlled laboratory study investigated the response and recovery potential of tubeworms to the high CO_2-induced changes of OA in terms of the effects on the structure of their tubes as the end product of the calcification process. Overall, the results support our hypothesis that the biofouling tube-forming serpulid polychaete tubeworm, *Hydroides elegans*, will be able to recover their calcifying potential upon returning to normal pH conditions after exposure to near-future OA levels. This is largely expected as this study species inhabits coastal environments with highly variable conditions, and they are also reported to have high levels of genetic variability within the population with sufficient plasticity to tolerate a wide range of environmental stressors including OA (Lane et al. 2015). Our study found that although the tubeworm is highly sensitive to near-future OA levels projected within this century, it is also resilient and would not only survive under

OA with structurally impaired and mechanically weaker tubes, but would also fully recover from these impacts once returned to normal pH environments. In the following sections, we discuss the results in the context of the calcification mechanism of tubeworms under OA and their implications on biofouling.

4.1 Calcification - potential plasticity to OA effects

The tubeworm is considered to be ecologically and economically important to biogenic reefs in coastal waters of tropical oceans. The adhesion strength of tubeworms (0.7 MPa) is several-fold higher than that of other biofouling species, such as barnacles (0.06 MPa) (Kavanagh et al. 2001). For example, the removal of fouling organisms from man-made structures (such as fishnets and cooling water pipelines) is made more challenging if the community is dominated by tubeworms (Kavanagh et al. 2001).

Under projected near-future decreased seawater pH of 7.8 and reduced carbonate ion saturation levels, tubeworms will form impaired tubes with poor mechanical properties and at a significantly slower rate (Chan et al. 2012; Li et al. 2014). This was confirmed in the present study, which found that relatively long-term exposure to decreased pH over 30 days (stage 1) resulted in this general trend, especially as tubeworms undergo rapid calcification in early-life stages.

In response to pH 7.8, tubeworms produced tubes with a higher calcite to aragonite ratio and with lower density packing (Figure 3a, 4a, and 5c-d). Tubes with altered mineral composition (in this study) and altered microstructure (Chan et al. 2012) result in mechanically weaker tubes. The mechanical modelling tests predicted that tubes produced at pH 7.8 would be more vulnerable to external pressures, such as predatory attacks (Li et al. 2014). These results indicate the calcification mechanisms, including the formation and transport of crystals to the site of

calcification, internal pH homeostasis, and allocation of more metabolic energy for calcification over other processes, would not produce mechanically strong tubes under decreased pH, although worms might survive but calcify at slower rates (Li et al. 2014). To the best of our knowledge, the force required to remove biofouling tubeworm communities with mechanically weaker tubes produced at decreased pH has yet to be estimated.

Not all biofouling species respond to decreased pH in the same way. For example, like tubeworms, spirorbid worms are also highly vulnerable to a pH of 7.7 (Peck et al. 2015), whereas barnacles respond to pH 7.4 by producing mechanically stronger shells that require a greater external pressure to break (McDonald et al. 2009). Similarly, the shell mechanical properties of juvenile eastern oysters are not affected by decreased pH and elevated pCO_2 (800 μatm) under optimal salinity (Dickinson et al. 2012). More importantly, the effects of decreased pH are dependent on other stressors in the environment including salinity and temperature. For example, the effects of decreased pH on tubeworms are reversed at elevated temperature (Chan et al. 2013; Li et al. 2016), whereas reduced salinity makes eastern oysters produce mechanically weaker shells at decreased pH. Multiple stressor experiments on biofouling species and mechanical measurements are necessary to study the effect of OA on biofouling communities, especially from the perspective of biofouling control (Chan et al. 2013; Li et al. 2016).

4.2 Recovery of tube mechanical properties after exposure to OA

This study showed that the biofouling calcareous tubeworm could survive at pH 7.8 with partially impaired and mechanically weakened tubes. Importantly, once they returned to a normal ambient pH environment, they were able to recover fully their tube chemical composition and mechanical properties. Notably, tubeworms showed a remarkable ability to restore their tube composition towards a lower calcite to aragonite ratio, resulting in greater mechanical resistance.

This result suggests that natural swings in environmental pH due to OA and other coastal processess such as algal production may provide them an opportunity to strengthen their protective tube structures. Similar to this finding, several coral species including *Cladocora caespitosa* (Movilla et al. 2012), *Oculina patagonica* (Fine & Tchernov 2007; Movilla et al. 2012), and *Madracis pharencis* (Fine & Tchernov 2007) have been shown to recover from OA impacts when returned to normal pH. In these coral species, calcification was reinstated when hypercapnic-induced metabolic changes were removed, as calcification can be a highly energy-consumptive process (Miles et al. 2007; Brewer & Peltzer 2009). The observed recovery from OA impacts by different species may be explained by potentially different calcification mechanisms that come into play when the carbonate system is altered (Holcomb et al. 2009; Ries 2011). For example, some species may have a greater pH-buffering capacity to raise the saturation state at the site of calcification gaining additional resilience and recovery potential in response to OA (McCulloch et al. 2012).

To the best of our knowledge, this is one of the few studies to measure tube mechanical properties as a function of the environmental pH (Figure 6). Interestingly, tubeworms exposed to decreased pH during stage 1 and 2 (TT group) had double the hardness and stiffness rates compared to the CC group. This unexpected result suggests that tubeworms in the TT group can counteract the effects of OA by acquiring higher robustness from a posterior to anterior direction of the tube compared to the CC group (Figures 6a and d). These findings are consistent with our previous studies that found early juvenile stages are more susceptible to the corrosive effect of OA, resulting in tubes with higher aragonite content and weaker mechanical strength, but in later developmental stages, they gradually obtain the capacity to counteract OA (Chan et al. 2012; Li et al. 2014). On the other hand, the positive threshold pattern observed in the TC group demonstrated their ability to recover their tube mechanical properties when returned to a normal pH environment (Figure

6c). Furthermore, the tube calcium polymorph ratio and mineral density changes due to decreased pH were reversed after switching back to the ambient pH (Figure 3b, 4b and 5e). The results from this study suggest that this specific tubeworm species in Hong Kong has adequate genetic diversity or physiological plasticity to survive large-scale pH and carbonate chemistry changes, which are projected to occur in current and near-future coastal oceans due to climate change.

4.3 Implications on fouling community development

This study suggests that certain subtropical populations of the dominant biofouling tubeworms, *Hydroides elegans*, have existing genetic diversity, physiological tolerance, plasticity, and importantly, the recovery ability to mitigate near-future OA levels. However, according to this study and other reports, OA is still able to cause significant damage to the tube mineral composition, structure and mechanical strength, which would make tubeworms more vulnerable to predators and other environmental stressors reducing their chance to recover before normal pH levels return. Therefore, both the duration of exposure to OA stress and the recovery ability of the dominant biofouling tubeworm should be considered as key factors when projecting the survival of biofouling communities under projected near-future decreased pH. Further studies are required to investigate the impact of OA and the recovery ability of tubeworms on biofouling community dynamics on substratum, and the consequences for antifouling paints, chemical and physical compositions.

Acknowledgements

The authors would like to thank Kelvin W. K. Yeung and Tony Liu of the Department of Orthopaedics and Traumatology, Li Ka Shing School of Medicine, University of Hong Kong for their help with the micro-CT work. This study was supported by GRF grants from the HKSAR-RGC (Grant Numbers: 17304914 and 17303517).

References

Asnaghi V, Mangialajo L, Gattuso J-P, Francour P, Privitera D, Chiantore M. 2014. Effects of ocean acidification and diet on thickness and carbonate elemental composition of the test of juvenile sea urchins. Mar Environ Res. 93:78-84.

Baumann H, Wallace RB, Tagliaferri T, Gobler CJ. 2015. Large Natural pH, CO_2 and O_2 Fluctuations in a Temperate Tidal Salt Marsh on Diel, Seasonal, and Interannual Time Scales. Estuar Coast. 38(1):220-231.

Beniash E, Ivanina A, Lieb NS, Kurochkin I, Sokolova IM. 2010. Elevated level of carbon dioxide affects metabolism and shell formation in oysters *Crassostrea virginica*. Mar Ecol Prog Ser. 419:95-108.

Borgesa AV, Gypensb N. 2010. Carbonate chemistry in the coastal zone responds more strongly to eutrophication than ocean acidification. Limnol Oceanogr. 55(1):346-353.

Brewer PG, Peltzer ET. 2009. Limits to Marine Life. Science. 324(5925):347-348.

Cai W-J, Hu X, Huang W-J, Murrell MC, Lehrter JC, Lohrenz SE, Chou W-C, Zhai W, Hollibaugh JT, Wang Y et al. 2011. Acidification of subsurface coastal waters enhanced by eutrophication. Nat Geosci. 4(11):766-770.

Celenk C, Celenk P. 2012. Bone density measurement using computed tomography. InTech.

Chan VBS, Li C, Lane AC, Wang Y, Lu X, Shih K, Zhang T, Thiyagarajan V. 2012. CO_2-driven ocean acidification alters and weakens integrity of the calcareous tubes produced by the serpulid tubeworm, *Hydroides elegans*. PloS ONE. 7(8):e42718.

Chan VBS, Thiyagarajan V, Lu XW, Zhang T, Shih K. 2013. Temperature dependent effects of elevated CO_2 on shell composition and mechanical properties of *Hydroides elegans*: insights from a multiple stressor experiment. PloS ONE. 8(11):e78945.

Clode PL, Lema K, Saunders M, Weiner S. 2011. Skeletal mineralogy of newly settling *Acropora millepora* (Scleractinia) coral recruits. Coral Reefs. 30(1):1-8.

Dickinson GH, Ivanina AV, Matoo OB, Portner HO, Lannig G, Bock C, Beniash E, Sokolova IM. 2012. Interactive effects of salinity and elevated CO_2 levels on juvenile eastern oysters, *Crassostrea virginica*. J Exp Biol. 215(1):29-43.

Dickinson GH, Matoo OB, Tourek RT, Sokolova IM, Beniash E. 2013. Environmental salinity modulates the effects of elevated CO_2 levels on juvenile hard-shell clams, *Mercenaria mercenaria*. J Exp Biol. 216(14):2607-2618.

Dickson AG, Millero FJ. 1987. A comparison of the equilibrium constants for the dissociation of carbonic acid in seawater media. Deep Sea Res (I Oceanogr Res Pap). 34(10):1733-1743.

Dobretsov, S., Coutinho, R., Rittschof, D., Salta, M., Ragazzola, F. and Hellio, C., 2019. The oceans are changing: impact of ocean warming and acidification on biofouling communities. Biofouling. 35(5):585-595.

Doerner MF, Nix WD. 1986. A method for interpreting the data from depth-sensing indentation instruments. J Mater Res. 1(4):601-609.

Doney SC, Fabry VJ, Feely RA, Kleypas JA. 2009. Ocean Acidification: The Other CO_2 Problem. Ann Rev Mar Sci. 1(1):169-192.

Duarte CM, Hendriks IE, Moore TS, Olsen YS, Steckbauer A, Ramajo L, Carstensen J, Trotter JA, McCulloch M. 2013. Is ocean acidification an ppen-ocean syndrome? Understanding anthropogenic impacts on seawater pH. Estuar Coast. 36(2):221-236.

Dupont S, Thorndyke M. 2009. Impact of CO_2-driven ocean acidification on invertebrates early life-history – What we know, what we need to know and what we can do. Biogeosci Disc. 6(2):3109-3131.

Espinel-Velasco N, Hoffmann L, Agüera A, Byrne M, Dupont S, Uthicke S, Webster NS, Lamare M. 2018. Effects of ocean acidification on the settlement and metamorphosis of marine invertebrate and fish larvae: a review. Mar Ecol Prog Ser. 606:237-257.

Feely RA, Orr J, Fabry VJ, Kleypas JA, Sabine CL, Langdon C. 2009. Present and future changes in seawater chemistry due to ocean acidification. Geophys Monogr Ser. 183:175-188.

Fine M, Tchernov D. 2007. Scleractinian Coral Species Survive and Recover from Decalcification. Science. 315(5820):1811-1811.

Fitridge I, Dempster T, Guenther J, de Nys R. 2012. The impact and control of biofouling in marine aquaculture: a review. Biofouling. 28(7):649-669.

Ghalambor CK, Mckay JK, Carroll SP, Reznick DN. 2007. Adaptive versus non-adaptive phenotypic plasticity and the potential for contemporary adaptation in new environments. Funct Ecol. 21(3):394-407.

Gienapp P, Teplitsky C, Alho JS, Mills JA, Merilä J. 2008. Climate change and evolution: disentangling environmental and genetic responses. Mol Ecol. 17(1):167-178.

Hendriks IE, Duarte CM, Olsen YS, Steckbauer A, Ramajo L, Moore TS, Trotter JA, McCulloch M. 2015. Biological mechanisms supporting adaptation to ocean acidification in coastal ecosystems. Estuar Coast Shelf Sci. 152:A1-A8.

Holcomb M, Cohen AL, Gabitov RI, Hutter JL. 2009. Compositional and morphological features of aragonite precipitated experimentally from seawater and biogenically by corals. Geochim Cosmochim Acta. 73(14):4166-4179.

Holcomb M, Venn AA, Tambutté E, Tambutté S, Allemand D, Trotter J, McCulloch M. 2014. Coral calcifying fluid pH dictates response to ocean acidification. Sci Rep. 4:5207.

Howarth R, Chan F, Conley DJ, Garnier J, Doney SC, Marino R, Billen G. 2011. Coupled biogeochemical cycles: eutrophication and hypoxia in temperate estuaries and coastal marine ecosystems. Front Ecol Environ. 9(1):18-26.

Ivanina AV, Falfushynska HI, Beniash E, Piontkivska H, Sokolova IM. 2017. Biomineralization-related specialization of hemocytes and mantle tissues of the Pacific oyster *Crassostrea gigas*. J Exp Biol. 220(18):3209-3221.

Kavanagh CJ, Schultz MP, Swain GW, Stein J, Truby K, Wood CD. 2001. Variation in adhesion strength of *Balanus eburneus*, *crassostrea virginica* and *hydroides dianthus* to fouling-release coatings. Biofouling. 17(2):155-167.

Lane AC, Campanati C, Dupont S, Thiyagarajan V. 2015. Trans-generational responses to low pH depend on parental gender in a calcifying tubeworm. Sci Rep. 5:10847.

Lane AC, Mukherjee J, Chan VBS, Thiyagarajan V. 2013. Decreased pH does not alter metamorphosis but compromises juvenile calcification of the tube worm. Mar Biol. 160(8):1983-1993.

Lannig G, Eilers S, Portner HO, Sokolova IM, Bock C. 2010. Impact of ocean acidification on energy metabolism of oyster, *Crassostrea gigas*-changes in metabolic pathways and thermal response. Mar Drugs. 8(8):2318-2339.

Li C, Chan VBS, He C, Meng Y, Yao H, Shih K, Thiyagarajan V. 2014. Weakening mechanisms of the serpulid tube in a high-CO_2 world. Environ Sci Technol. 48(24):14158-14167.

Li C, Meng Y, He C, Chan VBS, Yao H, Thiyagarajan V. 2016. Mechanical robustness of the calcareous tubeworm *Hydroides elegans*: warming mitigates the adverse effects of ocean acidification. Biofouling. 32(2):191-204.

McCulloch M, Falter J, Trotter J, Montagna P. 2012. Coral resilience to ocean acidification and global warming through pH up-regulation. Nat Clim Change. 2:623.

McDonald MR, McClintock JB, Amsler CD, Rittschof D, Angus RA, Orihuela B, Lutostanski K. 2009. Effects of ocean acidification over the life history of the barnacle *Amphibalanus amphitrite*. Mar Ecol Prog Ser. 385:179-187.

Mehrbach C, Culberson CH, Hawley JE, Pytkowicx RM. 1973. Measurement of the apparent dissociation constants of carbonic acid in seawater at atmospheric pressure. Limnol Oceanogr. 18(6):897-907.

Meng Y, Fitzer SC, Chung P, Li CY, Thiyagarajan V, Cusack M. 2018. Crystallographic Interdigitation in Oyster Shell Folia Enhances Material Strength. Cryst Growth Des. 18(7):3753-3761.

Meng Y, Guo Z, Fitzer SC, Upadhyay A, Chan VBS, Li C, Cusack M, Yao H, Yeung KWK, Thiyagarajan V. 2018. Ocean acidification reduces hardness and stiffness of the Portuguese oyster shell with impaired microstructure: a hierarchical analysis. Biogeosciences. 15(22):6833-6846.

Meng Y, Guo Z, Yao H, Yeung KWK, Thiyagarajan V. 2019. Calcium carbonate unit realignment under acidification: A potential compensatory mechanism in an edible estuarine oyster. Mar Pollut Bull. 139:141-149.

Miles H, Widdicombe S, Spicer JI, Hall-Spencer J. 2007. Effects of anthropogenic seawater acidification on acid-base balance in the sea urchin Psammechinus miliaris. Mar Pollut Bull. 54(1):89-96.

Movilla J, Calvo E, Pelejero C, Coma R, Serrano E, Fernández-Vallejo P, Ribes M. 2012. Calcification reduction and recovery in native and non-native Mediterranean corals in response to ocean acidification. J Exp Mar Bio Ecol. 438:144-153.

Nardone JA, Patel S, Siegel KR, Tedesco D, McNicholl CG, O'Malley J, Herrick J, Metzler RA, Orihuela B, Rittschof D et al. 2018. Assessing the Impacts of Ocean Acidification on Adhesion and Shell Formation in the Barnacle *Amphibalanus amphitrite*. Front Mar Sci. 5(369).

Oliver WC, Pharr GM. 1992. An improved technique for determining hardness and elastic modulus using load and displacement sensing indentation experiments. J Mater Res. 7(6):1564-1583.

Orr JC, Fabry VJ, Aumont O, Bopp L, Doney SC, Feely RA, Gnanadesikan A, Gruber N, Ishida A, Joos F. 2005. Anthropogenic ocean acidification over the twenty-first century and its impact on calcifying organisms. Nature. 437(7059):681-686.

Pansch C, Nasrolahi A, Appelhans YS, Wahl M. 2012. Impacts of ocean warming and acidification on the larval development of the barnacle *Amphibalanus improvisus*. J Exp Mar Bio Ecol. 420-421:48-55.

Peck LS, Clark MS, Power D, Reis J, Batista FM, Harper EM. 2015. Acidification effects on biofouling communities: winners and losers. Glob Chang Biol. 21(5):1907-1913.

Pierrot D, Lewis E, Wallace D. 2006. MS Excel program developed for CO_2 system calculations. ORNL/CDIAC-105a Carbon Dioxide Information Analysis Center, Oak Ridge National Laboratory, US Department of Energy, Oak Ridge, Tennessee.

Ries JB. 2011. Skeletal mineralogy in a high-CO_2 world. J Exp Mar Bio Ecol. 403(1–2):54-64.

Ries JB, Cohen AL, McCorkle DC. 2009. Marine calcifiers exhibit mixed responses to CO_2-induced ocean acidification. Geology. 37(12):1131-1134.

Solomon S, Qin D, Manning M, Averyt K, Marquis M. 2007. Climate change 2007-the physical science basis: Working group I contribution to the fourth assessment report of the IPCC. Vol. 4. Cambridge university press.

Tanur AE, Gunari N, Sullan RMA, Kavanagh CJ, Walker GC. 2010. Insights into the composition, morphology, and formation of the calcareous shell of the serpulid *Hydroides dianthus*. J Struct Biol. 169(2):145-160.

Thomsen J, Gutowska MA, Saphörster J, Heinemann A, Trübenbach K, Fietzke J, Hiebenthal C, Eisenhauer A, Körtzinger A, Wahl M et al. 2010. Calcifying invertebrates succeed in a naturally CO_2-rich coastal habitat but are threatened by high levels of future acidification. Biogeosciences. 7(11):3879-3891.

Toyofuku T, Matsuo MY, de Nooijer LJ, Nagai Y, Kawada S, Fujita K, Reichart G-J, Nomaki H, Tsuchiya M, Sakaguchi H et al. 2017. Proton pumping accompanies calcification in foraminifera. Nat Commun. 8:14145.

Underwood AJ. 1999. Physical disturbances and their direct effect on an indirect effect: responses of an intertidal assemblage to a severe storm. J Exp Mar Bio Ecol. 232(1):125-140.

Vinn O, Kirsimäe K, ten Hove HA. 2009. Tube ultrastructure of *Pomatoceros americanus* (Polychaeta, Serpulidae): Implications for the tube formation of serpulids. Est J Earth Sci. 58(2):148 - 152.

Vinn O, Kupriyanova EK. 2011. Evolution of a dense outer protective tube layer in serpulids (Polychaeta, Annelida). Carnets de géologie.137-147.

Watson DI, Shumway SE, Whitlatch RB. 2009. 13 - Biofouling and the shellfish industry. In: Shumway SE, Rodrick GE, editors. Shellfish Safety and Quality. Woodhead Publishing; p. 317-337.

Wood HL, Spicer JI, Widdicombe S. 2008. Ocean acidification may increase calcification rates, but at a cost. Proc R Soc Lond B Biol Sci. 275(1644):1767-1773.

Wootton JT, Pfister CA, Forester JD. 2008. Dynamic patterns and ecological impacts of declining ocean pH in a high-resolution multi-year dataset. Proc Natl Acad Sci. 105(48):18848-18853.

Yuan XC, Yin K, Cai WJ, Ho AY, Xu J, Harrison PJ. 2011. Influence of seasonal monsoons on net community production and CO_2 in subtropical Hong Kong coastal waters. Biogeosciences. 8(2):289-300.

Figure Legends

Figure 1 Schematic of the experimental design. The study was designed to have two stages, stage 1: 0-30 days and stage 2: 30-60 days. Tubeworms, *Hydroides elegans,* were cultured under control conditions (C, pH 8.1) and treatment conditions (T, pH 7.8). There were four groups with four replicates in each group: CC group (stage 1: pH 8.1, stage 2: pH 8.1), CT group (stage 1: pH 8.1, stage 2: pH 7.8), TC group (stage 1: pH 7.8, stage 2: pH 8.1), and TT group (stage 1: pH 7.8, stage 2: pH 7.8). (a) 3D tube construction showing the tube growth during stage 1 (grey) and stage 2 (white).

Figure 2 The tube length of *Hydroides elegans* during the two experimental stages. (a) The tube length during stage 1 in the control groups (pH 8.1) and the treatment groups (pH 7.8). (b) The tube length during stage 2 in the CC group (stage 1: pH 8.1, stage 2: pH 8.1) and TC group (stage 1: pH 7.8, stage 2: pH 8.1) (mean ± SD).

Figure 3 The tube calcite/aragonite ratio of *Hydroides elegans* quantified by X-ray diffraction (XRD) analysis. (a) The calcite/aragonite ratio in tube sections during stage 1 of the control groups (pH 8.1) and the treatment groups (pH 7.8). (b) The calcite/aragonite ratio in tube sections during stage 2 in the CC group (stage 1: pH 8.1, stage 2: pH 8.1) and TC group (stage 1: pH 7.8, stage 2: pH 8.1) (mean ± SD).

Figure 4 Tube compositions of *Hydroides elegans* detected by Fourier transform infrared spectroscopy (FTIR). (a) The infrared absorption spectra obtained from tube sections during stage 1 (the black line represents the control group and the red line represents the treatment group). (b) The infrared absorption spectra obtained from tube sections during stage 2 (the black line represents the CC group and the green line represents the TC group). Abbreviations: A: aragonite peaks; C: calcite peaks; A/C: co-existing aragonite and calcite peaks; MO: organic matter peaks.

Figure 5 3D reconstruction models of the calcareous tubes of *Hydroides elegans* under each treatment (CC, CT, TC, TT) obtained from the micro-CT analysis (red colour = low density; white colour = high density). (a) Original 3D tube reconstructions, (b) 3D tube constructions with full density map, and (c) 3D tube constructions with only high-density portions (density > 0.5 g/cm^3).

The mineral density of tubes from (d) stage 1 and (e) stage 2 are presented in a bar chart (mean ± SD).

Figure 6 Nanoindentation results of the normalized hardness (left column) and stiffness (right column) over the normalized depth of 0 to 1 (0 = anterior opening; 1 = posterior end) of the calcareous tubes of *Hydroides elegans*. The four treatment groups were (a) CC group (stage 1: pH 8.1, stage 2: pH 8.1), (b) CT group (stage 1: pH 8.1, stage 2: pH 7.8), (c) TC group (stage 1: pH 7.8, stage 2: pH 8.1) and (d) TT group (stage 1: pH 7.8, stage 2: pH 7.8). Black solid lines show the best-fitting regressions.

Figure 1

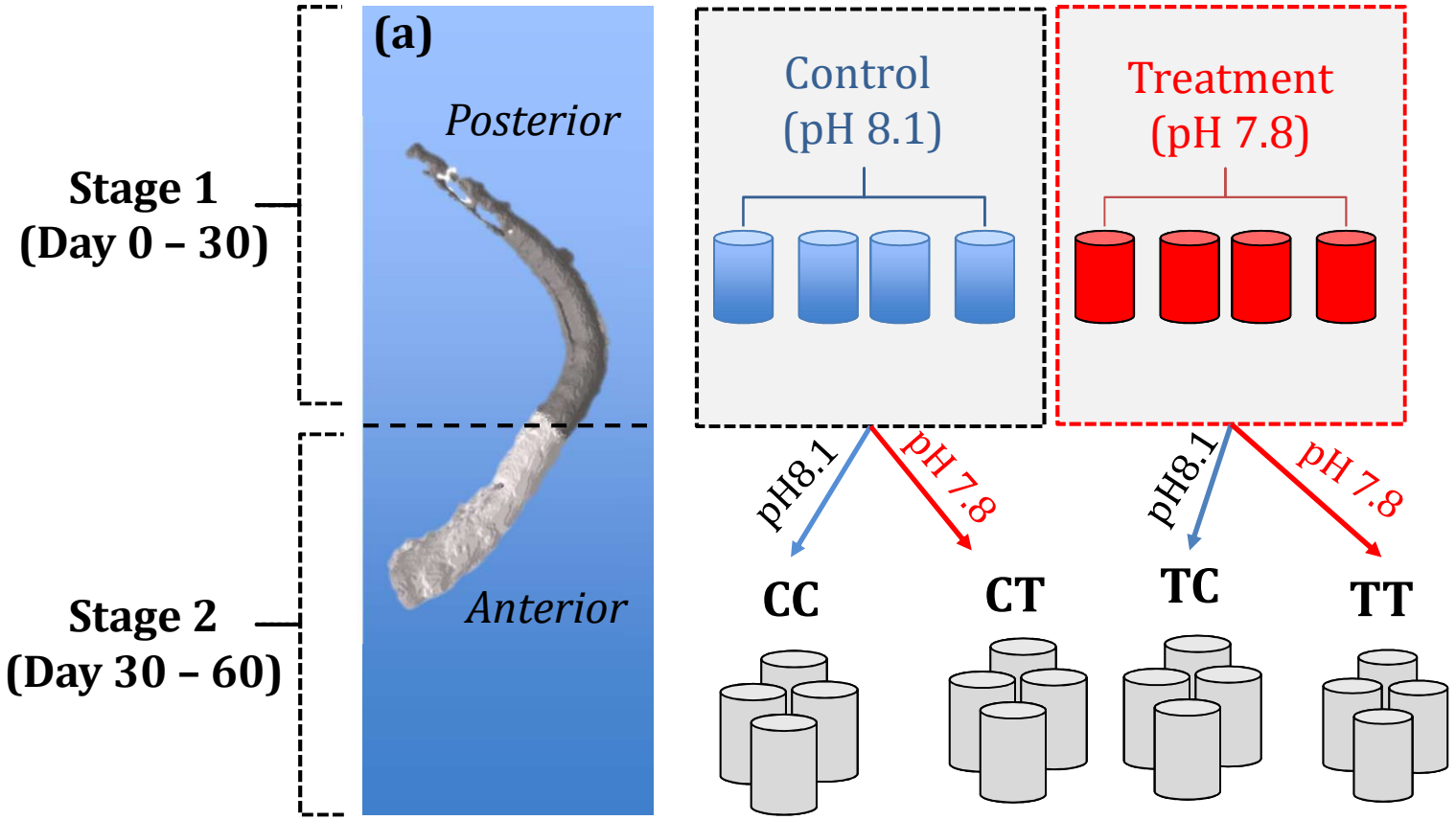
(a)
Posterior
Anterior
Stage 1
(Day 0 – 30)
Stage 2
(Day 30 – 60)
Control
(pH 8.1)
Treatment
(pH 7.8)
pH8.1
pH 7.8
pH8.1
pH 7.8
CC
CT
TC
TT

Figure 2

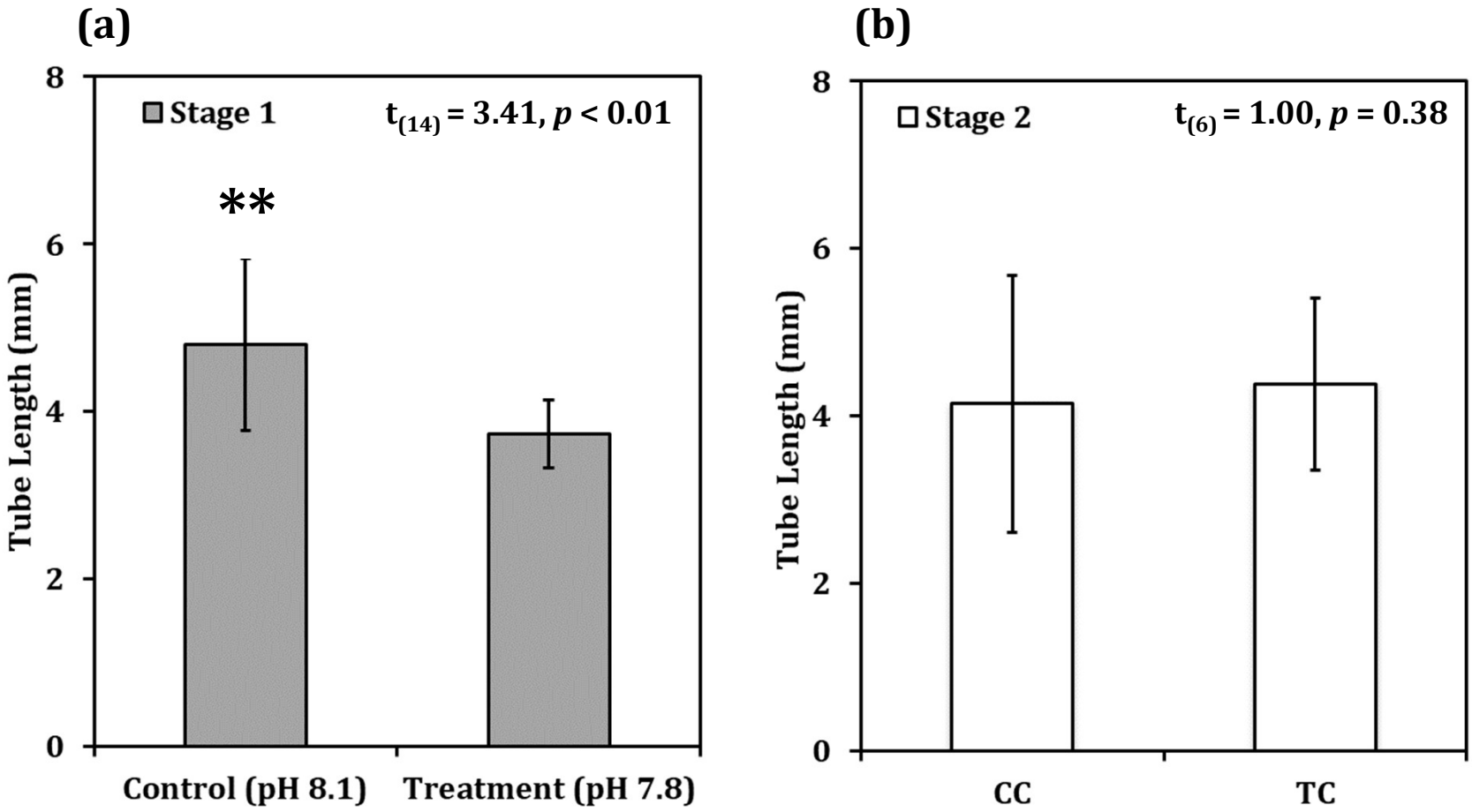
(a)
Stage 1
$t_{(14)} = 3.41, p < 0.01$
**
Tube Length (mm)
0
2
4
6
8
Control (pH 8.1)
Treatment (pH 7.8)
(b)
Stage 2
$t_{(6)} = 1.00, p = 0.38$
Tube Length (mm)
0
2
4
6
8
CC
TC

Figure 3

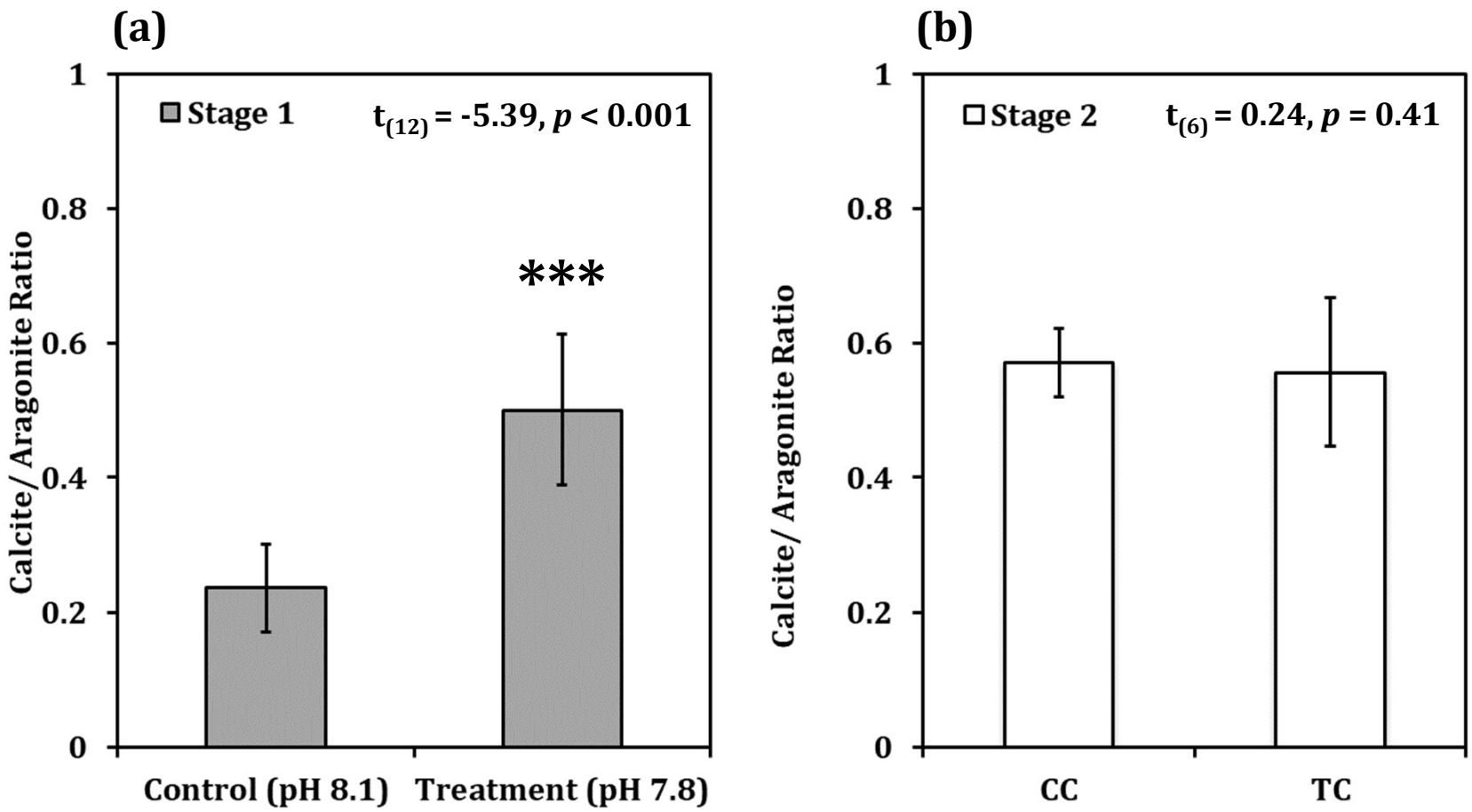
(a)
Stage 1
$t_{(12)} = -5.39, p < 0.001$
***
Calcite/ Aragonite Ratio
1
0.8
0.6
0.4
0.2
0
Control (pH 8.1)
Treatment (pH 7.8)
(b)
Stage 2
$t_{(6)} = 0.24, p = 0.41$
Calcite/ Aragonite Ratio
1
0.8
0.6
0.4
0.2
0
CC
TC

Figure 4

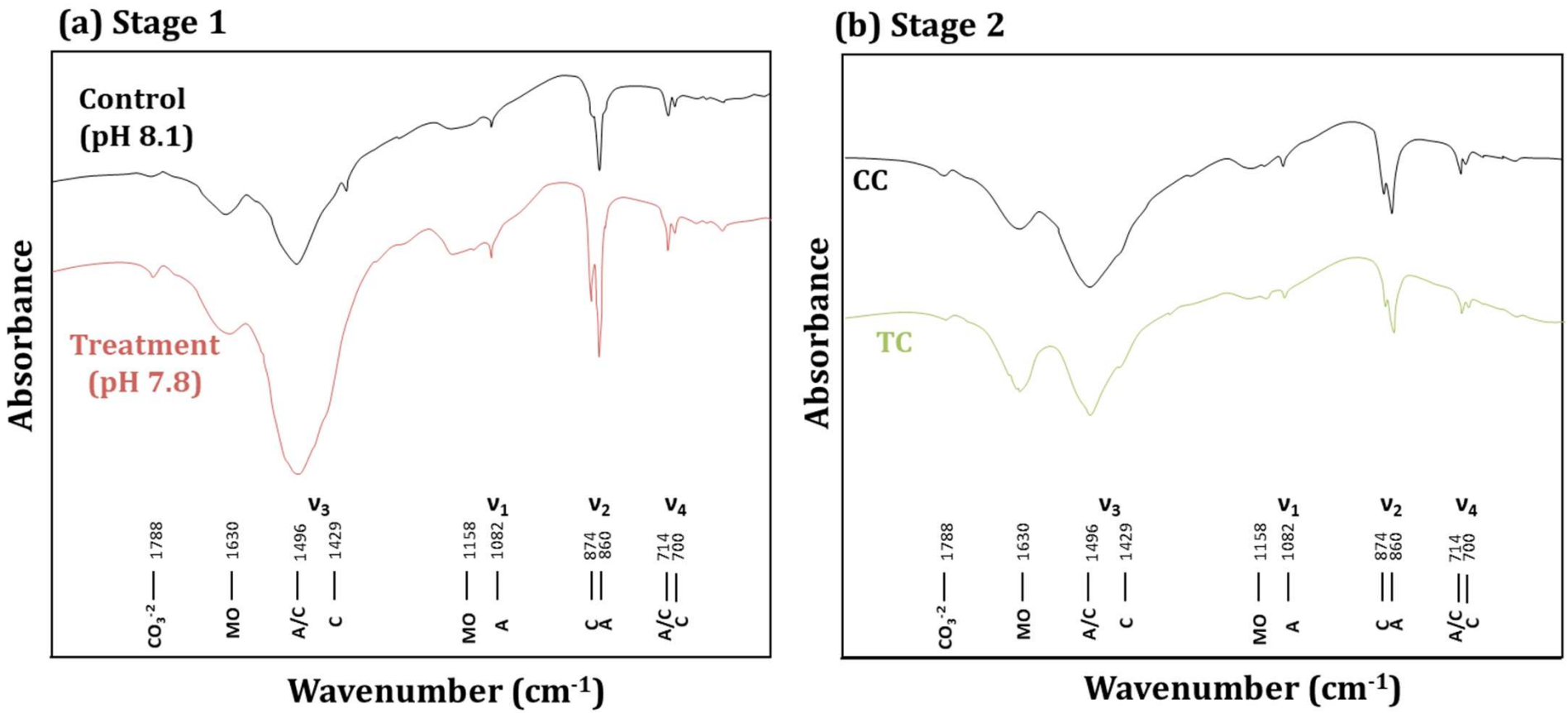
(a) Stage 1
Control
(pH 8.1)
Treatment
(pH 7.8)
Absorbance
CO_3^{-2} — 1788
MO — 1630
A/C — 1496
C — 1429
MO — 1158
A — 1082
C — 874
A — 860
A/C — 714
C — 700
ν_3
ν_1
ν_2
ν_4
Wavenumber (cm^{-1})
(b) Stage 2
CC
TC
Absorbance
CO_3^{-2} — 1788
MO — 1630
A/C — 1496
C — 1429
MO — 1158
A — 1082
C — 874
A — 860
A/C — 714
C — 700
ν_3
ν_1
ν_2
ν_4
Wavenumber (cm^{-1})

Figure 5

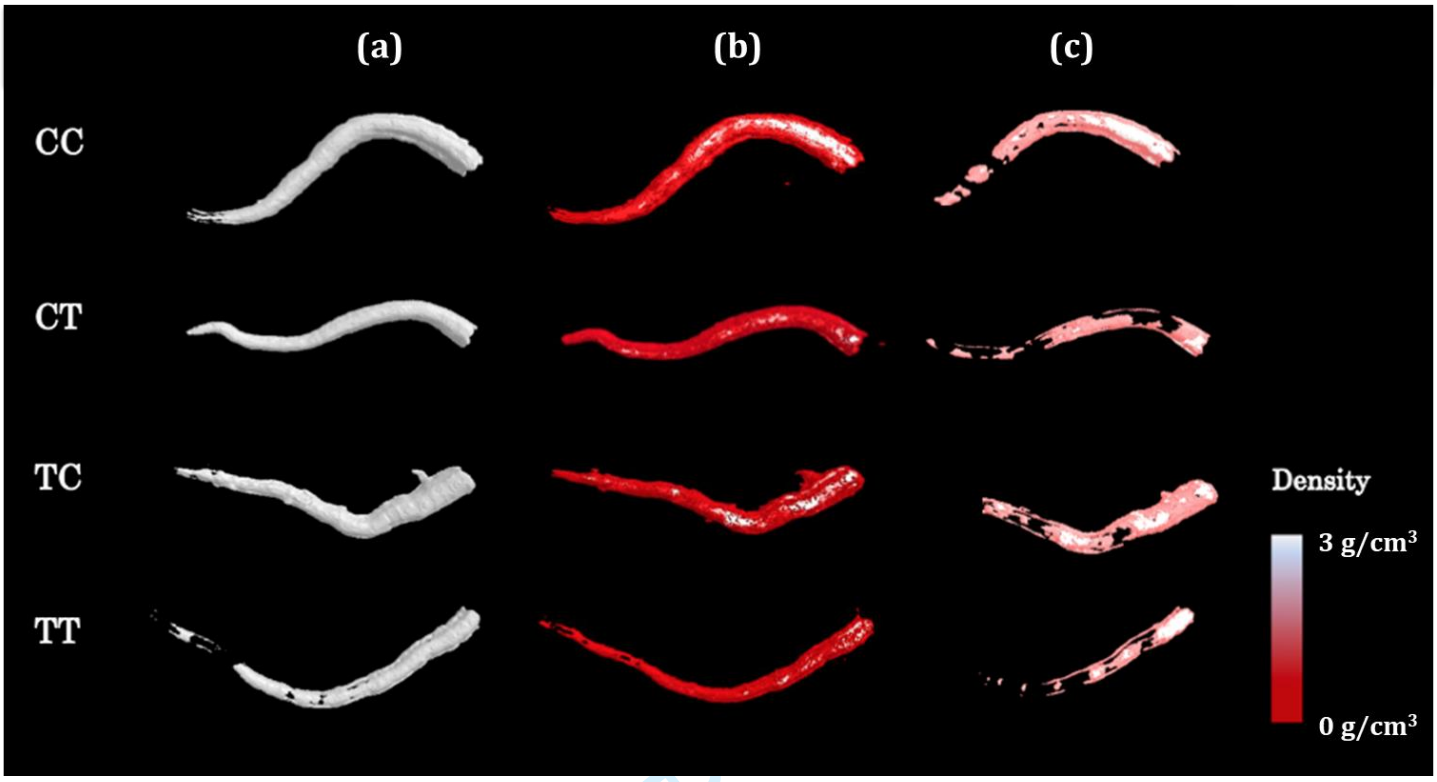
(a)
(b)
(c)
CC
CT
TC
TT
Density
3 g/cm³
0 g/cm³

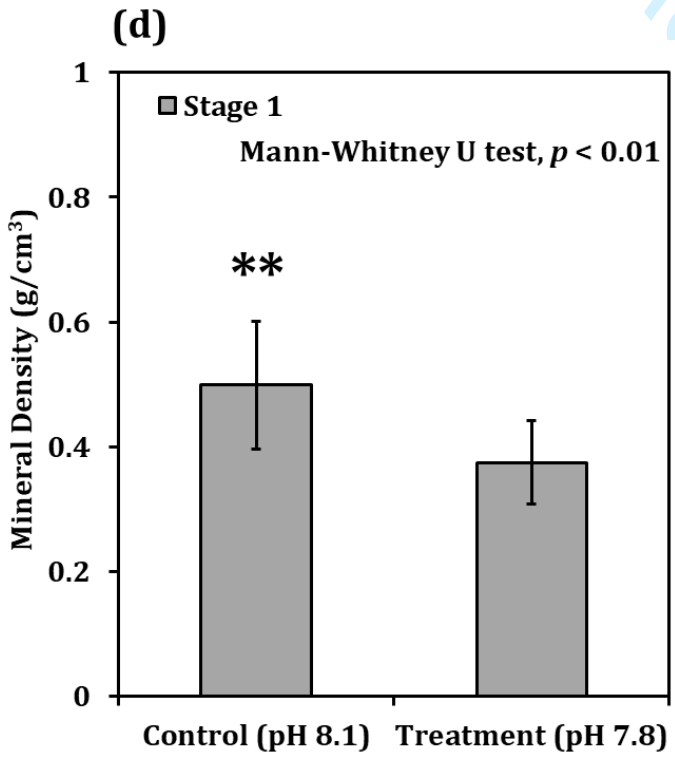
(d)
Stage 1
Mann-Whitney U test, p < 0.01
**
Mineral Density (g/cm³)
1
0.8
0.6
0.4
0.2
0
Control (pH 8.1)
Treatment (pH 7.8)

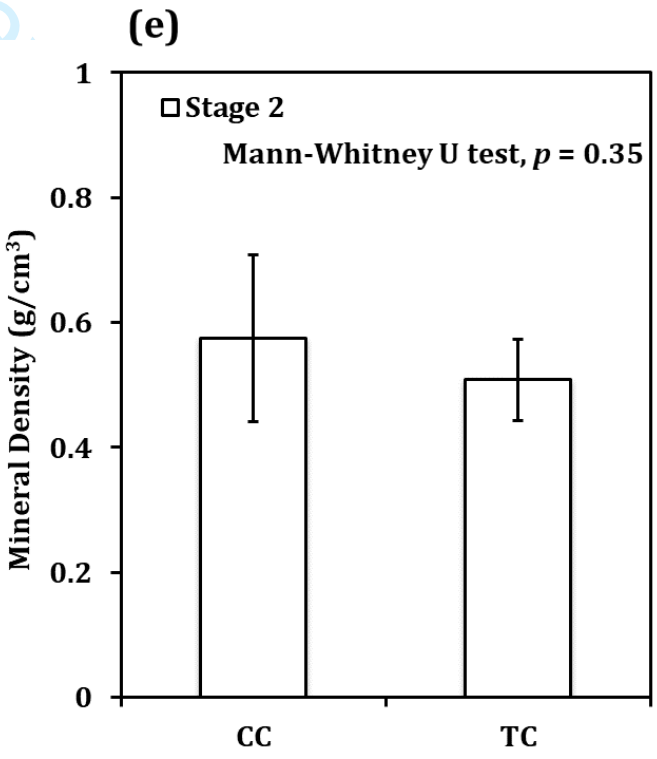
(e)
Stage 2
Mann-Whitney U test, p = 0.35
Mineral Density (g/cm³)
1
0.8
0.6
0.4
0.2
0
CC
TC

Figure 6

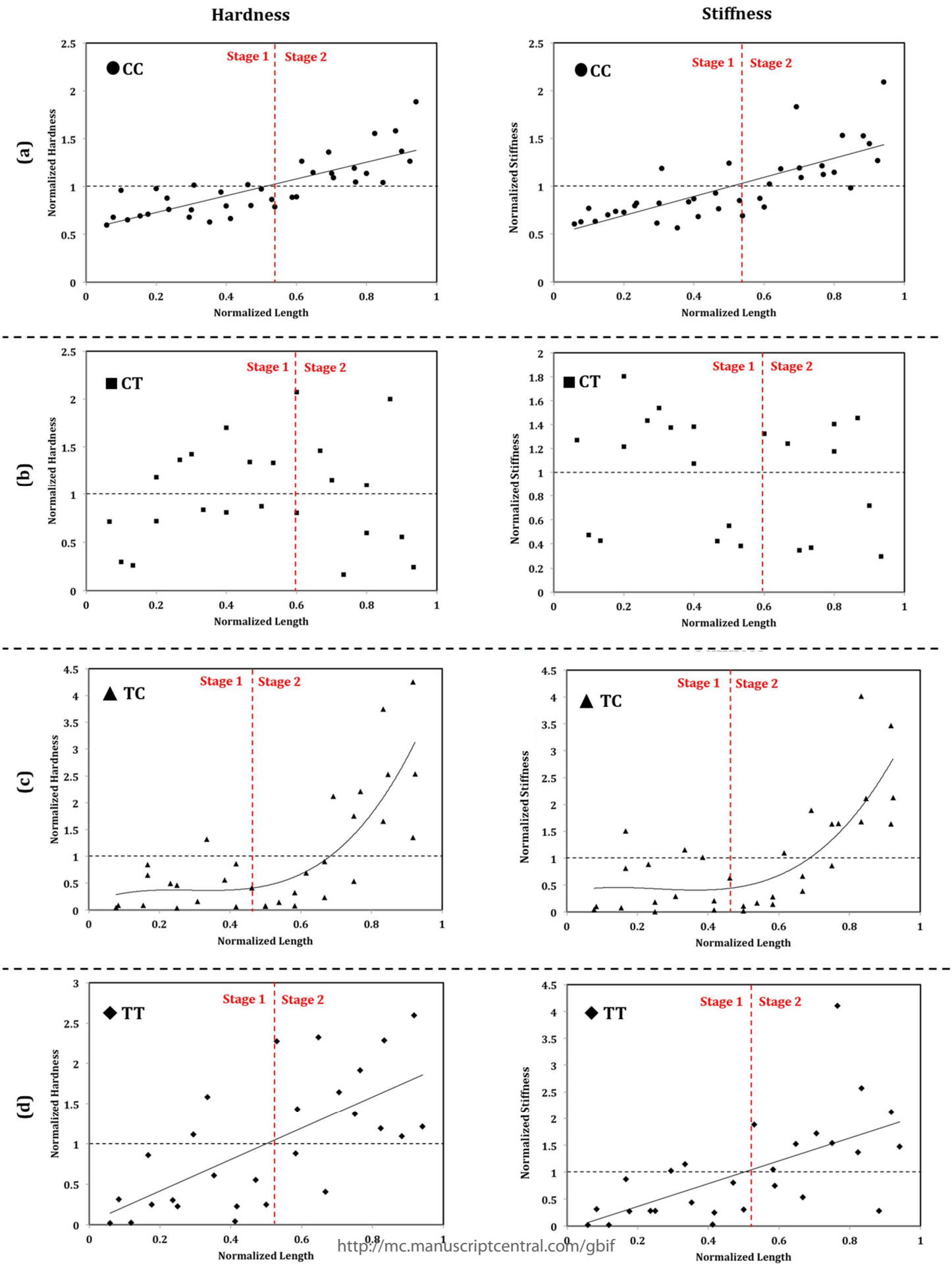
Hardness
Stiffness
(a)
(b)
(c)
(d)
CC
CT
TC
TT
Stage 1
Stage 2
Normalized Hardness
Normalized Stiffness
Normalized Length

Supplementary Materials

Recoverable impacts of ocean acidification on the tubeworm, *Hydroides elegans*: implication for biofouling in future coastal oceans

Yuan Meng[a], Chaoyi Li[a], Hangkong Li[b], Kaimin Shih[b], Chong He[c], Haimin Yao[c] and V. Thiyagarajan[a,d]*

[a]*The Swire Institute of Marine Science and School of Biological Sciences,* [b]*Department of Civil Engineering, The University of Hong Kong, Hong Kong SAR, China;* [c]*Department of Mechanical Engineering, The Hong Kong Polytechnic University, Hong Kong SAR, China;* [d]*State Key Laboratory for Marine Pollution, Hong Kong SAR, China*

*Corresponding author (V. Thiyagarajan: rajan@hku.hk)

Table S1. Measured and calculated values (mean ± SD; n = 4) of carbonate system parameters in culture tanks. Parameter abbreviations: pCO_2: partial pressure of carbon dioxide; CO_3^{2-}: carbonate ion concentration; $\Omega_{aragonite}$: aragonite saturation state; $\Omega_{calcite}$: calcite saturation state and TA: total alkalinity. Treatment abbreviations: C: pH 8.1 in stage 1; T: pH 7.8 in stage 1; CC: pH 8.1 in stage 1 and stage 2; CT: pH 8.1 in stage 1 and pH 7.8 in stage 2; TC: pH 7.8 in stage 1 and pH 8.1 in stage 2; TT: pH 7.8 in stage 1 and stage 2. 2 main stages in the experimental design: stage 1: 0-30 days ("0" denotes the time when the worms settled) and stage 2: 30-60 days.

Measured parameters						Calculated parameters			
Stage 1	**Stage 2**	**pH**	**Salinity (psu)**	**Temperature (°C)**	**TA (µequiv kg^{-1})**	**pCO_2 (µatm)**	**CO_3^{2-} (µmol kg^{-1})**	**$\Omega_{calcite}$**	**$\Omega_{aragonite}$**
C	**CC/TC**	8.09 ±0.01	34.0±0.1	22.5±0.1	2128±101	478±31	153.3±4	3.71±0.11	2.42±0.07
T	**CT/TT**	7.80±0.01	34.0±0.1	22.5±0.1	2152±92	1012±41	86.3±4	2.09±0.10	1.36±0.07

Table S2. Summary of the comparison on tube length, C/A ratio and density of stage 1 sections between CC and CT, and between TC and TT by using (a) student's t test and (b) Mann-Whitney U Test.

a. T-test Statistics

	t	df	*p*
Length			
CC vs CT	0.44	6	0.67
TT vs TC	0.29	6	0.77
C/A ratio			
CC vs CT	1.81	5	0.07
TT vs TC	-1.02	5	0.18
Density			
CC vs CT	-1.12	11	0.14

b. Mann-Whitney U Test

Density	
TT vs TC	$p = 0.27$

Table S3 Regression analyses of mechanical patterns (normalized hardness and stiffness) along the normalized length of the tubes from the CC, CT, TC and TT groups.

	Best-fit Regression				Response
	Regression	**Type**	***p***	**R^2**	
Hardness					
CC	$y = 0.88x + 0.55$	Linear	< 0.001	0.64	Positive
CT	No significant trend ($p>0.05$)	None	n/a	n/a	Neutral
TC	$y = 11.11x^3 - 9.65x^2 + 2.69x + 0.13$	Exponential	< 0.001	0.65	Threshold-positive
TT	$y = 1.94x + 0.03$	Linear	< 0.001	0.45	Positive
Stiffness					
CC	$y = x + 0.50$	Linear	< 0.001	0.58	Positive
CT	No significant trend ($p>0.05$)	None	n/a	n/a	Neutral
TC	$y = 8.85x^3 - 6.75x^2 + 1.39x + 0.37$	Exponential	< 0.001	0.60	Threshold-positive
TT	$y = 2.12x - 0.06$	Linear	< 0.001	0.38	Positive